

# Compression properties of cost-efficient porous expanded clay reinforced AA7075 syntactic foams fabricated by industrial-oriented die casting technology

\*İsmail Cem Akgün<sup>1</sup>, Çağın Bolat<sup>2</sup>, and Ali Gökşenli<sup>1</sup>

1. Faculty of Mechanical Engineering, Istanbul Technical University, 34437, İstanbul, Turkey

2. Faculty of Engineering, Samsun University, 55420, Samsun, Turkey

Copyright © 2024 Foundry Journal Agency

**Abstract:** In today's manufacturing industries, hard competition between rival firms makes it compulsory for researchers to design lighter and cheaper machine components due to the megatrends of cost-effectiveness and anti-pollution. At this point, aluminum syntactic foams (ASFs) are new-generation engineering composites and come into the upfront as a problem-solver. Owing to their features like low density, sufficient elongation, and perfect energy absorption ability, these advanced foams have been considerably seductive for many industrial sectors nowadays. In this study, an industrial-oriented automatic die casting technology was used for the first time to manufacture the combination of AA7075/porous expanded clay (PEC). Micro evaluations (optical and FESEM) reveal that there is a homogenous particle distribution in the foam samples, and inspections are compatible with the other ASF studies. Additionally, T6 aging heat treatment was operated on one half of the produced foams to explore the probable impact of aging on the compressive responses. Attained results show that PEC particles can be an alternative to expensive hollow spheres used in the previous works. Besides, a favorable relationship is ascertained between the aging treatment and mechanical properties such as compression strength and plateau strength.

**Keywords:** die casting; porous materials; metal matrix syntactic foams; expanded clay; compressive deformation

CLC numbers: TG146.21

Document code: A

Article ID: 1672-6421(2024)01-060-11

## 1 Introduction

Aluminum foams are new-generation metallic materials that have one main phase: an aluminum metal matrix with different-sized inner pores. Recently, these interesting materials have become attractive for researchers owing to their perfect compressive properties, considerably low density, high specific strength, and good impact/energy absorption capability<sup>[1-4]</sup>. Along with the rising demand for engineering foams, other alternative closed-cell

metallic foams emerge, aiming to solve mechanical problems such as high energy absorption, specific compression strength, and impact strength. At this point, aluminum composite foams, or in other words aluminum syntactic foams (ASFs), come to the forefront.

Metallic syntactic foams can be interpreted also as composite foams that utilize a reinforcement particle to create inner gap volume. Compared to conventional foams, ASFs possess numerous advantages<sup>[3, 5]</sup>. The main advantage of ASFs is the control of inner gap size, amount, and shape providing a constricted density range. In addition, reinforcement particles contribute to total mechanical strength values in a positive manner. Thanks to these properties, ASFs are considered great alternatives for conventional foams and composites.

When the reinforcement particles are taken into consideration, thin-walled/hollow ceramic-based granules<sup>[6]</sup>, glass-based micro-scaled spheres<sup>[7]</sup>, fly

\*İsmail Cem Akgün

Research assistant. His research interests are mainly focused on metal syntactic foams, casting technologies, and the mechanical behavior of metals. He has various scientific publications dealing with aluminum syntactic foams, die casting of metal matrix syntactic foams, and machinability of composite foams.

E-mail: akgunism@itu.edu.tr

Received: 2023-07-28; Accepted: 2023-12-11

ash cenospheres<sup>[8]</sup> and metallic hollow beads<sup>[9]</sup> can be noticed from the scholarly archives. Herein, especially hollow spheres and micro-scale glasses are highly expensive materials. As for the metallic steel spheres, these fillers can be described as performance-booster, but they raise the total density compared to their ceramic rivals. Recently, to hinder that kind of handicaps, some other alternative cellular structures (expanded clay, expanded glass, pumice, and expanded perlite) were tried to balance the cost and performance. In addition, on the sectoral basis, ASFs are target materials for lots of industrial sectors like automotive, aviation, building/construction, marine, transportation/railway, and biomedical applications<sup>[3, 10, 11, 12]</sup>.

Aluminum alloys are generally selected as a metallic matrix in syntactic foam manufacturing due to their relatively low density ( $2.7\text{--}2.8\text{ g}\cdot\text{cm}^{-3}$ ) and frequent utilization in lots of industrial branches. For example, Al alloys have been examined with dissimilar reinforcement particles to ascertain mechanical behaviors and failure characteristics elaborately<sup>[13-15]</sup>. Thalmaier et al.<sup>[16]</sup> offered a novel production technique called spark plasma sintering for the manufacturing of expanded perlite-added aluminum foams and emphasized that up to 57% levels could be achieved for inner porosity. Movahedi et al.<sup>[17]</sup> analyzed the impact behavior of A356 Al matrix syntactic foams and pointed out that dynamic strengthening was observed under the impact loading. In another research, Akgün et al.<sup>[18]</sup> revealed that AA7075/expanded glass syntactic foams could be produced through a novel sandwich infiltration casting and homogenous particle distribution, and better compressive properties could be created. Aside from these valuable investigations, many researchers focused on heat treatment of ASFs due to their widespread preferability in numerous sectoral implementations and suitability for heat treatment procedures for mechanical properties enhancement. Rao et al.<sup>[19]</sup> performed different heat treatments on reinforced AA7055 matrix syntactic foam samples and stated that energy absorption capacity and plateau strength values of the produced foams increased after heat treatment. Movahedi et al.<sup>[20]</sup> examined possible influences of the heat treatment process on expanded perlite reinforced ZA27 alloy syntactic foam and declared that thermal cycles improved the specific energy absorption ability, plateau stress levels, and energy absorption efficiency of fabricated products. Similar developments in the mechanical responses were recorded also by Balch et al.<sup>[21]</sup> for T6-treated ceramic microsphere reinforced AA7075 syntactic foam. Besides, in another work, Santa et al.<sup>[22]</sup> exerted to conceive the impacts of different heat treatment processes (T4 and T7 treatment) on the damage characteristics of  $\text{Al}_2\text{O}_3$  reinforced aluminum syntactic foam. The investigation group noted that heat-treated products displayed higher average peak strength than their non-treated alternatives.

Various fabrication methods have been developed to produce ASFs. For example, the sintering-oriented powder metallurgical method is one of the candidates. However, compaction-resistant, expensive and hard fillers should be used in this method as the risk of reinforcement breakage is a significant handicap<sup>[23-26]</sup>.

Through the stir-mixing method, ceramic granules are blended in the molten aluminum matrix. In spite of its application easiness and process cheapness, the most apparent drawbacks of the stir-mixing method are that thin-walled hollow spheres may damage with impact effects and a nonuniform inner structure may arise. In this work, our project team propounded a new idea with an industrial production technique called cold chamber die casting to obtain a good bonding harmony between Al matrix/porous expanded clay (PEC) particles as well as the precise product dimensions, industrial-oriented cold chamber die casting technology is offered for syntactic foam fabrication in this work due to its perfect ability to adapt to automation and rapid production capacity.

The main goal of this study is to show the production possibility of Al matrix/porous expanded clay composite foam system via an industrial-oriented die casting technology, and to figure out the effect of T6 treatment on the compressive responses and damage styles of ASFs fabricated via a novel asserted die casting technology. In the experimental effort, the AA7075 series of aluminum was used as matrix metal because of its common usage in the target sectors and serious potential for artificial aging process. As for reinforcement ceramics, PEC granules were preferred by reason of their unique cellular/porous structure and relative cheapness. After die casting, T6 artificial aging thermal treatment was implemented in some of the fabricated ASFs to check its effect on mechanical properties. Moreover, macroscopic and microscopic inspections were done and uniaxial quasi-static compression tests were carried out to comprehend the detailed mechanical features.

## 2 Methods and materials

### 2.1 Main constituents of ASFs

Al-Zn (7075) ingots were catered via Güray Aluminum Limited Company (Istanbul, Turkey). From the supplier knowledge, the matrix metal includes 5.68wt.% Zn, 2.39wt.% Mg, 1.4wt.% Cu, 0.21wt.% Fe, 0.2wt.% Si, 0.18wt.% Mn, 0.034wt.% Ti and 0.018wt.% Zr. As for filler material, LECAT<sup>®</sup> expanded clay spheres with a grain size of 2–4 mm produced by Söğüt Toprak Madencilik Sanayi Inc. (Ankara, Turkey) were used. The chemical composition of the spheres is 64.83wt.%  $\text{SiO}_2$ , 15.05wt.%  $\text{Al}_2\text{O}_3$ , 7.45wt.%  $\text{Fe}_2\text{O}_3$ , 3.67wt.% MgO, 2.98wt.% CaO, 2.55wt.%  $\text{K}_2\text{O}$ , 1.1wt.%  $\text{Na}_2\text{O}$ , 0.63wt.%  $\text{TiO}_2$ , 0.13wt.%  $\text{P}_2\text{O}_5$ , 0.13wt.% MnO and the 1.37wt.% ignition loss. Due to high accessibility on Turkish domestic market and low costs, PEC with a low average bulk density ( $0.613\text{ g}\cdot\text{cm}^{-3}$ ) and high sintering temperature ( $650\text{ }^\circ\text{C}$ ) can be a great alternative material in metal syntactic foam production. In the aspect of the mechanical response, the PEC particles used in this study exhibit an average crush strength of 5.2 MPa according to the EN 13055 standard. Besides, rough surface of PEC particles ascends the surface area of the particles so it will increase the wettability of the PEC particle surfaces, which makes the production processes of metallic syntactic foams easier.

During the manufacturing processes and/or transportation,

PEC particles may break, and possess undesired fragments, and different ceramic dust. Therefore, before the die-casting process, PEC particles were cleaned manually at first, and then were carefully filtered with a proper sieve, and the granule size interval was tried to keep constant between 2–4 mm.

### 2.2 Die casting procedure of ASFs

One of the well-known industrial metal casting processes, automatic cold chamber die casting, was used to achieve the production of ASFs. The primary aim of the method is to have properly filled mold cavity to form a homogenous foam structure. The secondary aim of the method is to repeat the production process rapidly in order to mass production of ASFs with minimum effort and have more standardized products. At the first stage of production process, the shot sleeve and steel mold of the die-casting machine was heated up to 230 °C via a resistance wire heating element installed around the mold system after the lubrication process. For lubrication, Trewa-S die release agent was applied inside the mold. Then, a little piece of thin aluminum foil was placed on the mold entrance for holding the PEC particles inside the mold cavity. Otherwise, the PEC particles would fill the die inlet between the mold cavity and shot chamber and restrain the aluminum flow into the mold. Another advantage of the lubrication was to hold the aluminum thin foil piece on the bottom surface of the die. Then, the PEC particles were filled into the mold up to 7/8th height of the mold (115 cm<sup>3</sup>) to give the particles more space and free path to move. The more mold cavity was packed (more height of PEC particles), the harder it would be to inject the molten aluminum into the mold and penetrate between the particles. Meanwhile, the less mold

cavity packed (less height of PEC particles) would ascend the density of foam products. PEC particles were preheated to 400 °C for 20 min to prevent molten aluminum to solidify earlier than it desired to be. Furthermore, the mold cavity was closed with a steel lid and the preparation of the mold was completed. After the mold was closed, the machine turned on and starting point of injection cylinder was set. Following this operation, graphite crucible was taken from the induction furnace, and molten aluminum at 800 °C was poured into the shot chamber. Immediately after "Start" command was given to the system via the start button, the injection cylinder injected the molten aluminum into the mold cavity with 30 MPa pressure and at 40 mm·s<sup>-1</sup> speed. The machine held the pressure for 10 s after the movement of the injection cylinder was completed. Following this sequence, injection cylinder turned back to the starting position and production process was finished. Finally, the steel lid was removed, the movable die was taken backwards and the product was ejected from mold cavity. Figure 1 demonstrates the production step schematics of ASFs with die casting method.

The fabricated samples can be seen in Fig. 2. The height of the cylindrical samples varied between 75.86 mm and 78.3 mm while diameter values were 44.5±0.1 mm. Before the mechanical tests, all samples were cleaned, grinded, and polished sensitively.

To analyze the effect of heat treatment on the mechanical properties and fracture mechanism, T6 heat treatment was performed on some selected specimens. Samples were heated to 480 °C, held for 2 h followed by water quenching. Aging process was carried out at 120 °C for 24 h.

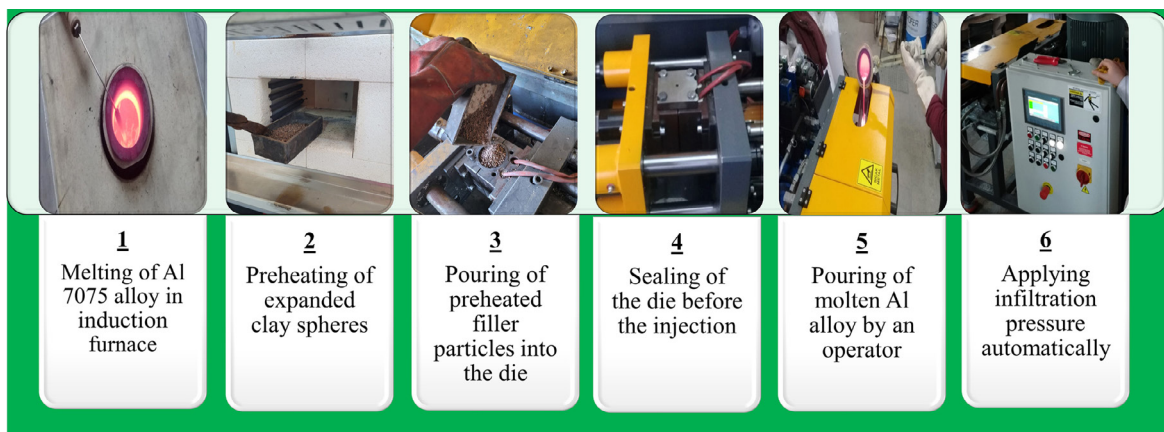


Fig. 1: Production steps of ASF via die casting



Fig. 2: ASF sample with PEC filler particles

### 2.3 Characterization of manufactured ASFs

During the microscopic evaluations of the PEC particles and produced ASF samples, a fused emission scanning electron microscope (FESEM), and a Nikon SMZ800 model optical microscope with DpxView-Pro software were used for microstructure observation. Before microstructural observations, foam samples were sliced with cutter equipment and subjected to a grinding process using 180–1000 grit with SiC emery papers in a Metcon Forcipol 2V machine. Then,

the polishing process was conducted using 1 μm diamond suspension (Metcon Diapat). After that, polished foam samples were cleaned ultrasonically to sweep micron-sized contaminations or dirty sediments.

For physical calculations and characterization, density of the syntactic foam ( $\varphi_{SF}$ ) samples was determined by recorded the Eq. (1):

$$\varphi_{SF} = \frac{m_{SF}}{V_{SF}} \quad (1)$$

where,  $V_{SF}$  is the volume of the sample and  $m_{SF}$  is the mass of the sample. The mass of the samples was measured using a precision scale (Precisa XB220A) with an accuracy of ± 0.0001 g.

To assess the volume fraction of PEC particles ( $F_{fil}$ ) and average porosity amount ( $F_{TP}$ ), mathematical equations propounded by Taherishargh [27] were taken:

$$F_{fil} = \left[ \left( V_{syn} - \left( \frac{m_{syn} - m_{fil}}{\rho_{alu}} \right) \right) \frac{1}{V_{syn}} \right] \times 100 \quad (2)$$

$$\rho_{fil} = \frac{m_{fil}}{V_{syn} - \left( \frac{m_{syn} - m_{fil}}{\rho_{alu}} \right)} \quad (3)$$

$$F_{TP} = F_{fil} \left[ 1 - \frac{\rho_{fil}}{\rho_{sd}} \right] \quad (4)$$

where,  $V_{syn}$ ,  $m_{syn}$ ,  $m_{fil}$ ,  $\rho_{fil}$ ,  $\rho_{alu}$  and  $\rho_{sd}$  are the syntactic foam volume, foam mass, mass of PEC particles, particle density of PEC, density of the matrix, and density of solid-state of the PEC particles respectively.

Compressive responses of the ASF samples were appointed using a computer-controlled 600 kN Dartec uniaxial testing machine cooperating with MTS Station Manager data acquisition software. Throughout the tests, the force and displacement data were recorded and altered to engineering stress-engineering strain values by utilizing initial foam height and initial cross-sectional area. In addition, test speed remained constant at 1 mm·min<sup>-1</sup> during the compression deformation. To increase the test accuracy, a lubricant was used on compression plate surfaces prior to all tests to provide uniform uniaxial force distribution and to prevent the ductile barreling effect. Furthermore, all tests were recorded with a digital camera to better understand the damage mechanism of the samples.

For examination of mechanical responses, compressive strength (1% yield strength), plateau stress, plateau-end strain, densification strain energy absorption, and energy absorption efficiency values were calculated from the stress-strain data in accordance with ISO 13314 standard [28]. Firstly, the slope of the linear region was used to determine compressive strength values. To identify plateau stress values, the arithmetic mean of the calculated stress values between 0.2 and 0.4 engineering strain was utilized through the data provided by MTS Station Manager software. Plateau-end strain (densification strain) value was the value on which the engineering stress value

equals 1.3 times the measured plateau stress. In terms of the energy absorption values ( $W$ ), data collected from the stress-strain curves was integrated up to 0.5 engineering strain. Finally, the energy absorption efficiency ( $\eta$ ) was calculated by using Eq. (6):

$$W = \int_0^{0.5} \sigma d\varepsilon \quad (5)$$

$$\eta = \frac{W}{\sigma_{max} \times 0.5} \quad (6)$$

where  $\sigma_{max}$  is the maximum compressive stress up to 50% strain.

## 3 Results and discussion

### 3.1 Manufactured ASFs and its physical properties

Figure 3 shows that the PEC particles are in a sphere-like shape and majorly in closed form. Additionally, the inner cellular structure can be seen in detail in Fig. 4. This micro-image indicates comprehensive FESEM views of the inner cell struts and the outer surface of the PEC particles. This structure consists of different-sized and non-uniform cells.

The characteristic microstructure of the produced ASFs [Fig. 5] is consistent with previous literatures for the MSFs [3, 29]. According to Fig. 5, it can be found that a homogeneous two-phased syntactic structure is created successfully due to the high speed/high-pressure casting ability of the industrial-oriented die casting. Meanwhile, even in quite narrow gaps [Fig. 5(a)], successful metal penetration between PEC granules is obtained. Some PEC particles tend to adhere to each other, as illustrated in Fig. 5(a). This circumstance can be interpreted as local thermal sintering and observed partially in all ASFs. Apart from this case, some small casting pits resulting from Al metal shrinkage in the solidification step are observed, as demonstrated in Fig. 5(b). These pits may form around the Al matrix/PEC interface throughout the solidification owing to the different thermal conductivity between the PEC granules and the AA7075 metal. Furthermore, no penetration of the molten metal into the PEC particles is found.

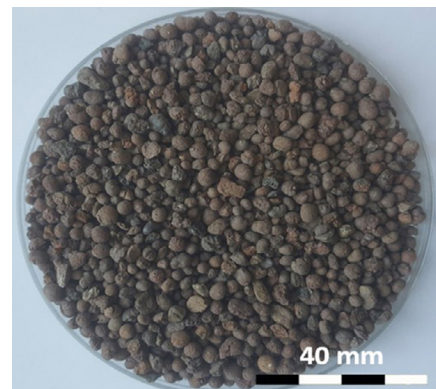


Fig. 3: Macro photograph of PEC granules

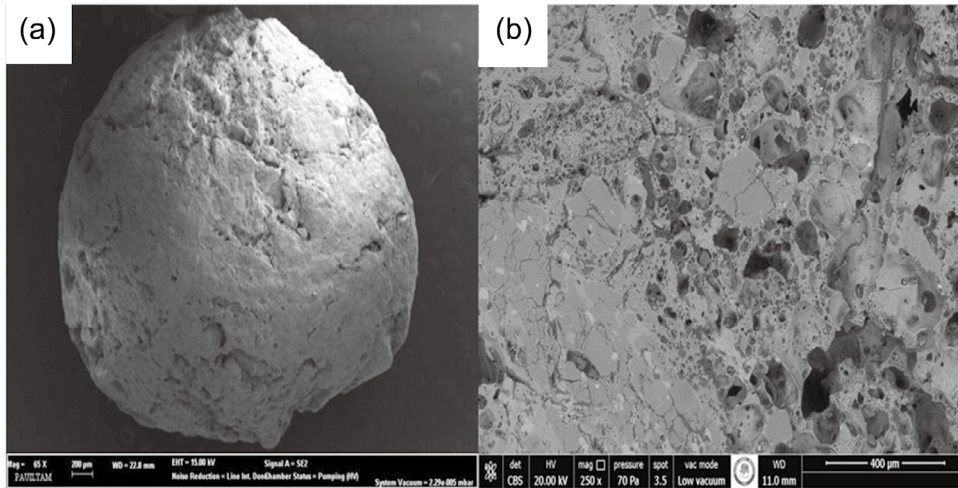


Fig. 4: SEM images of PEC particle (a) and inner porous structure (b)

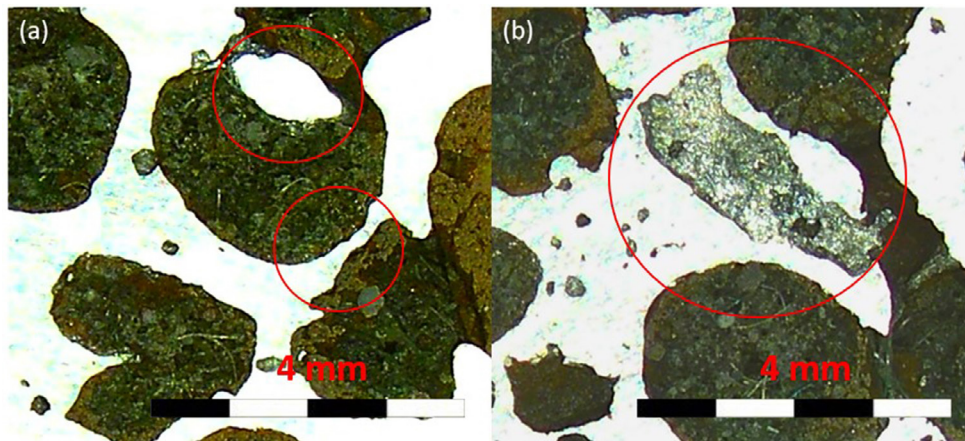


Fig. 5: Microscopic images of manufactured ASFs: (a) infiltration between narrow; (b) channelsand casting pits

The volume fraction of reinforcement granules ( $F_{fi}$ ) and total porosity of the foam samples ( $F_{Tp}$ ) were calculated using Eqs. (2–4). Related results are list in Table 1. In Table 1, as-cast and their aged versions are grouped in doubles as SF1-SF2 (T6), SF3-SF4 (T6), SF5-SF6 (T6), and SF7-SF8 (T6). In this categorization, the factor of the close density level was adopted.

The density values of the produced samples range between 1.89 and 1.92  $\text{g}\cdot\text{cm}^{-3}$ . This is consistent with other literature works and can be evaluated as a medium-top density segment compared to other metallic syntactic foams [3, 29, 30]. The design of industrial die casting, which focuses on filling the die cavity, enables the efficient placement of cellular PEC granules into the die cavity prior to the casting process,

Table 1: Physical properties of produced ASFs

Sample	Height (mm)	Diameter (mm)	Density ( $\text{g}\cdot\text{cm}^{-3}$ )	Filler volume (%)	Total porosity (%)
SF1	76.94	44.48	1.89	69.29	35.61
SF2-T6	76.56	44.53	1.90	69.20	35.43
SF3	76.71	44.57	1.91	68.43	34.78
SF4-T6	75.86	44.60	1.92	68.72	34.74
SF5	76.13	44.59	1.93	68.22	34.34
SF6-T6	78.01	44.48	1.93	67.36	34.14
SF7	77.05	44.63	1.94	67.18	33.77
SF8-T6	78.30	44.60	1.95	66.20	33.28

leading to a decrease in the density of the metal foam. In general, PEC granules are majorly rigid and brittle ceramics and have various small-sized pores that induce low fracture toughness in their solid structures. Besides, SiO<sub>2</sub>-based PEC particles are more fragile than metal matrix. In fact, both deformed reinforcements and Al metal leakage into the reinforcement materials can be considered undesired cases because of the fact that they lead to density rising and can dominate the damage mechanism of the ASFs due to increase of metal matrix, which has higher density than the reinforcement material. Meanwhile, if they are compared with PEC particles, certain thin-walled hollow spheres like special ceramic mixtures and glass microspheres are more sensitive to rapid breakage and liquid metal penetration [26, 29, 31, 32]. According to the results in Table 1, porosity levels stay between a narrow range of 33.28%–35.61%. What's more, executing heat treatment does not have an influence on the average density and total porosity of the ASFs.

### 3.2 Mechanical properties of ASFs

Obtained compressive engineering stress-engineering strain graphs of as-cast and T6 aging-treated ASFs are shown in Figs. 6 and 7, respectively. In Figs. 6 and 7, the observed stress-strain graphs reflect characteristic stress-strain behavior of ASFs that is well defined in the literature [3, 20, 30]. An elastic-based

linear deformation area can be found at the initial stages of the deformation. After the engineering stress values reach the peak point, they drop slightly, and a characteristic plateau zone begins. In the plateau zone, measured engineering stress values oscillate, and continuous plastic deformation occurs in the Al matrix. This region is significant for ASFs, especially when target industries require enhanced energy absorption capacity. In the final stage of the compression tests, most of the reinforcement PEC particles are crashed, and engineering stress values rise abruptly owing to declining porosity.

Table 2 gives the mechanical test results.  $\sigma_{cmp}$ ,  $\sigma_{pl}$ ,  $\epsilon_{dsf}$ , and  $W$  refer to compression strength, plateau stress, plateau end strain, and energy absorption values respectively.

As-cast aluminium alloys exhibit poorer yield strength when they are compared with the T6 aging-treated alloys [33]. The situation is the same for ASFs since the Al metal matrix bears most of the mechanical load throughout deformation. Thus, yield strength levels of aging-treated syntactic samples surpass the related levels designated for as-cast samples at similar density/porosity values for all test samples. PEC particles can be taken as a weak phase to contribute to the mechanical features of the ASFs. The average compressive strength values of as-cast and aging-treated samples are 83.37 and 150.47 MPa, respectively. Besides, plateau strength is another term playing an important role to resist compressive deformation during

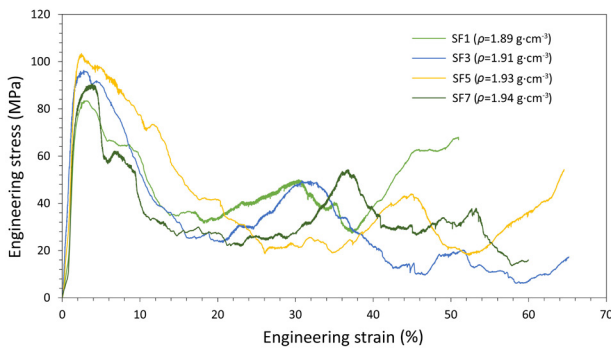


Fig. 6: Compressive stress-strain curves of as-cast produced syntactic foams depending on different average density values

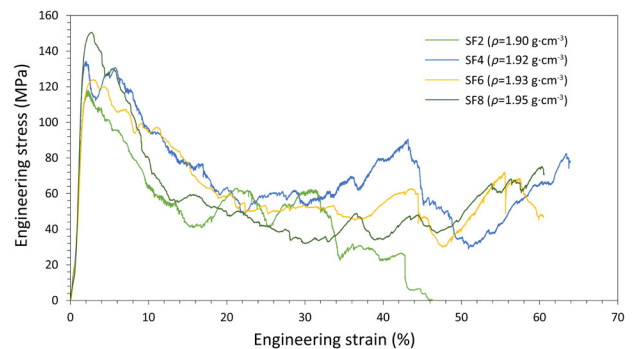


Fig. 7: Compressive stress-strain curves of T6 heat-treated syntactic foams depending on different average density values

Table 2: Compression features of manufactured ASFs

Foam No.	$\sigma_{cmp}$ (MPa)	$\sigma_{pl}$ (MPa)	$\epsilon_{dsf}$ (-)	$W$ (MJ·m <sup>-3</sup> )
SF1	83.37	41.28	0.50	37.27
SF2-T6	117.81	59.04	0.47	31.11
SF3	95.81	35.94	0.65	27.25
SF4-T6	134.29	54.55	0.64	57.49
SF5	102.96	31.79	0.65	31.63
SF6-T6	124.03	55.90	0.60	39.85
SF7	90.04	27.37	0.60	38.53
SF8-T6	150.47	40.72	0.61	35.72

large-strain deformation and for the capability of energy absorption. As same as the yield strength results, the plateau stress values of aging-treated foams are superior to their non-treated counterparts. The highest plateau value of 59.04 MPa belongs to the aging-treated samples. Aging-treated ASFs usually display better or equal performance in point of energy absorption capacity when compared with as-cast samples. This can be attributed to the random gap/cell structure of the PEC particles and the evolution of damage characteristics resulting from the aging-treatment of tested samples, which exhibit increased sensitivity to rising matrix strength and decreased matrix toughness. The highest calculated average energy absorption level is read for aging-treated foams as  $57.49 \text{ MJ}\cdot\text{m}^{-3}$  (the lowest average value of  $27.25 \text{ MJ}\cdot\text{m}^{-3}$  for as-cast samples). In addition, the specific correlation between aging treatment and plateau-end strain value is not established, despite the fact that the T6 treatment causes an increase in the

brittleness of the matrix. The average plateau-end strain values vary between 0.47 and 0.65 for all samples. Figure 8 shows the relationship between the mechanical properties and density levels.

In the light of the previous technical studies performed on metallic syntactic, there is a conceptual approach that compressive responses of the samples enhance with their ascending density levels [2]. Nevertheless, occasionally, little minor differences might be come across among nearly the identical or close density samples, so a likely answer for this is the heterogenous distribution of filler particles in the primary metal matrix together with the non-uniform outer diameter and cell form of the reinforcement ceramics. Moreover, in certain conditions, mechanical anisotropy due to the randomly cellular form of reinforcement particles might be observed. In Fig. 8, tested samples are compared to each other to see the positive effect of heat treatment on the compressive properties.

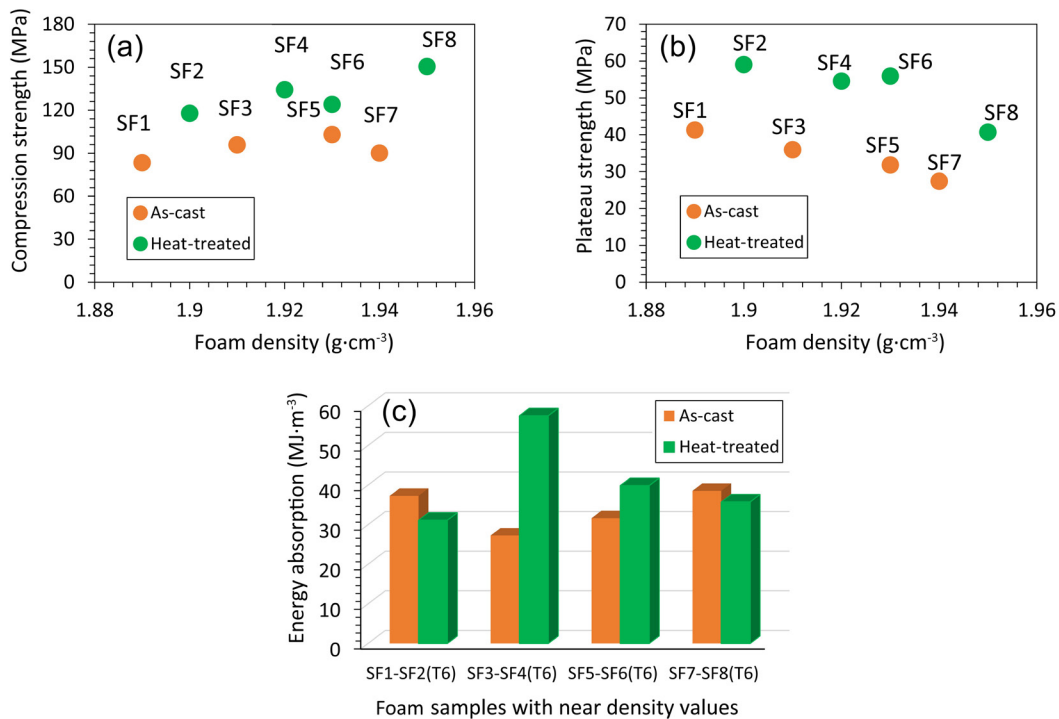
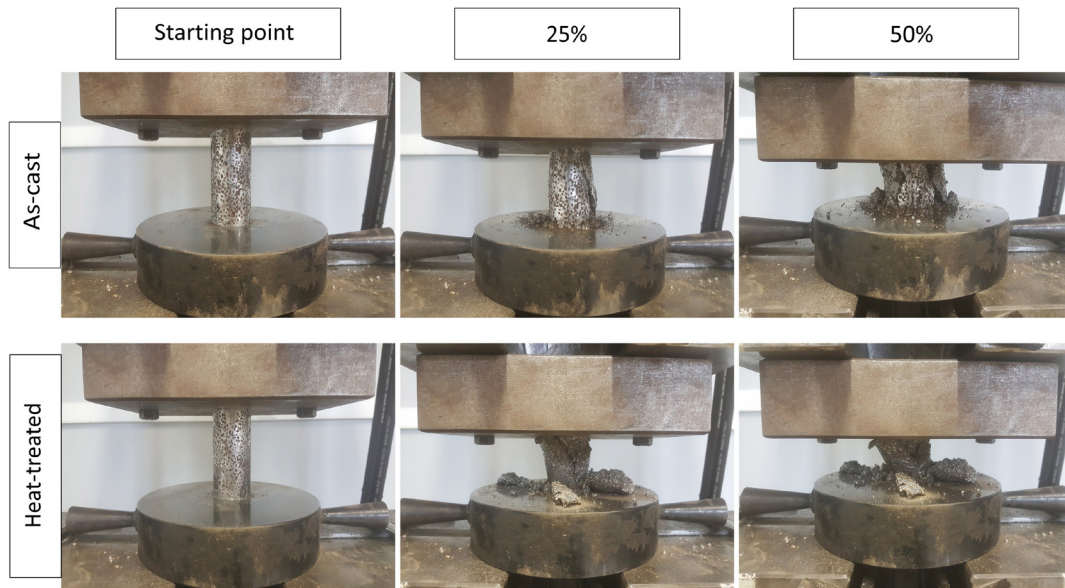


Fig. 8: Density-based mechanical features of as-cast and aging-treated foams: (a) compressive strength; (b) plateau stress; (c) energy absorption

### 3.3 Analysis of damage mechanisms

According to the previously published investigations [10, 11, 18, 20, 27], different kinds of damage behaviors are probable for ASFs depending on the Al alloy type, reinforcement ceramic granules, physical/chemical harmony among the main phases, manufacturing technology, and heat treatment. At this point, it is seen that if the plastic flow strength of the metal phase exceeds the breakage strength of the reinforcement granules, the dominant damage characteristic is observed as ductile-style deformation. Nevertheless, if the reinforcement breakage strength is greater than the plastic flow endurance of the metal phase, brittle dominant damage is effective in the damage style of the foams.

Figure 9 shows the macro-scale photos captured throughout the deformation of PEC-reinforced ASFs with ascending engineering strain percentages. At the initial stages, as-cast samples deform in an elastic manner and there is no evident shape change on the foam body. To further deformation, plastic flow mechanisms activate, and samples begin to damage plastically as a result of the climbing compressive force levels that reach the yield point of the Al metal. At 25% engineering strain, the ductile-based characteristic barreling effect becomes substantially apparent on the bottom-middle sections of the foam volume and the top sections that can also be identified as dead (almost non-damaged) sections stay un-deformed on a large scale. This observation can be explained by the



**Fig. 9: Deformation progress of the manufactured ASFs under compression loading depending on increasing engineering strain percentage**

presence of a porosity gradient in the cylindrical sample and the higher inner gap volume ratio in middle regions. For all as-cast samples, it is noticed that part regions possessing more porosity damage owing to compressive stress conglomeration. Starting from this stage of the mechanical tests and up to 50% strain, the deformation mechanism of the foam samples can be defined as hybrid-type damage (ductile barreling and brittle surface cracks). At 50% deformation, the number of surface cracks and brittle-style damaged zones increases till the end of the test. This can also be monitored in the plateau areas of the stress/strain curves in which the relatively flat zones represent the ductile behavior while the fluctuating zones (apparent peak-valley style or small oscillations) show the brittle body cracks.

Similar with the case observed for as-cast samples, the T6 aging-treated samples damage elastically in the early periods of the compressive loading and since the aluminum matrix and

PEC particles deform together, a rapid rising in the engineering stress values is seen in Fig. 7. In the peak stress value, there is a noteworthy difference for T6-treated samples, and their yield strength is greater than that of the as-cast foams because of the dislocation hindering capacity of secondary precipitates in the metal phase. At 25% deformation, in contrast with the as-cast foams, the T6-treated foams exhibit brittle dominant hybrid-type damage style, and this behavior continues in the large part of plastic deformation. Due to the combined effect of the strengthened metal sections with aging, localized merged PEC particles, and metal penetration into the PEC cell rooms, crack propagation is easier and faster for the T6-treated samples (Fig. 10). Also, the liquid metal penetration into the PEC particles can be explained by outer pores detected on the granule surfaces and FESEM observations given in Fig. 11 verify these discontinuities. Immediately after the 25% strain, separated foam sections can be distinguished and this is

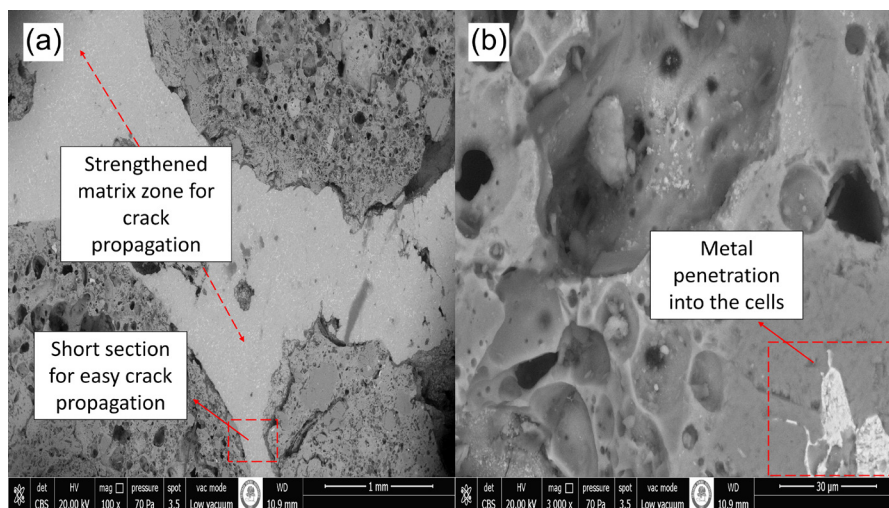


**Fig. 10: FESEM views of aging-treated samples: (a) matrix-rich section with narrow penetration zones; (b) metal penetration into PEC particles**

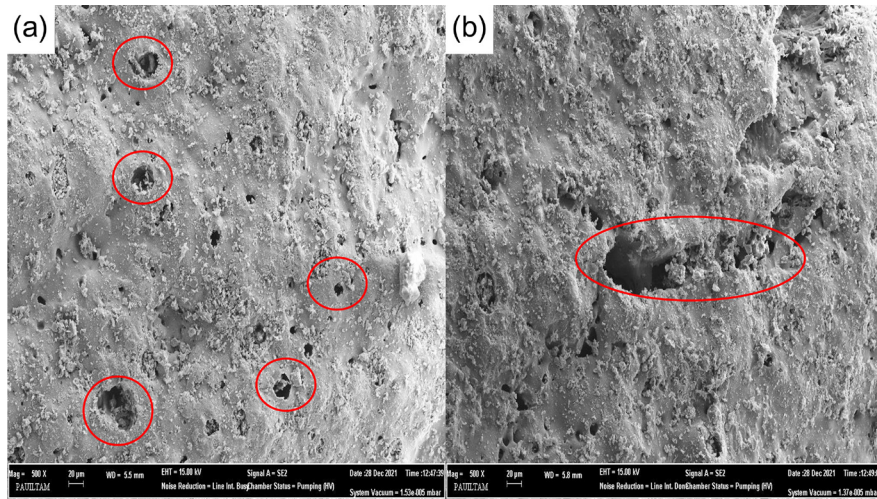


Fig. 11: FESEM views of PEC surface: (a) sphere-like small pits; (b) slot-like cavities

strongly related to the aging treatment that stimulating the matrix brittleness. As the deformation closes to 50% level, this brittle characteristic can be seen easily and discrete multiple cracks possessing diversified lengths and orientations become more evident. In addition, a little amount of ductile-based barreling is present in the top sections of the foams. Different-oriented surface or body cracks existed in the aging-treated foams can be accounted for escalated strength level and dwindling fracture toughness of the matrix metal of AA7075. Besides, as same as that happened in the as-cast samples, the plateau zone has certain oscillations in the T6-treated foams as a consequence of multiple crack propagation points, and supportive observations are also experienced by Bolat et al [13], and Fiedler et al [34].

Even sufficient filtration can be obtained in narrow intervals due to the industrial-oriented die-casting technology, this advantage only applies to the non-treated foams to prevent crack penetration, not to heat-treated foams owing to the age hardening effect. Different from the T6-treated foams, emerged cracks move rapidly in the cellular PEC granules, but these high-speed cracks can be decreased by the ductile Al metal phase. This situation is different for the aging-treated foams due to the metal matrix having relatively low fracture toughness. Aging-treated foams tend to loss their mono block integrity after the mechanical force is removed. At the end, as shown in Fig. 12, the initial foam body separates lots of independent fragments which can be seen around the big-sized fragments.

## 4 Conclusions

Considering all results collected from this experimental-based work regarding PEC particles reinforced AA7075 matrix syntactic foams, some featured findings can be listed:

(1) It is possible and applicable to fabricate PEC (with a grain size of 2–4 mm) reinforced AA7075 metallic syntactic foams through the newly proposed industrial-oriented die casting technology. For the near future, this technology is the

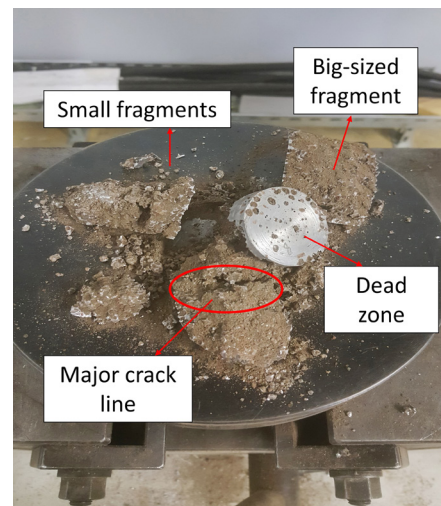


Fig. 12: Image of aging-treated sample after deformation

most remarkable candidate to produce machine parts including ASFs. Also, relatively big dimensions can be attained by this automatized die casting technology in comparison with the lab-scale methods used in the previous literature efforts.

(2) Aging treatment can improve mechanical properties of ASFs. Due to age-hardening influence and constrained dislocation movement in the metal phase, compressive strength of the aging-treated foams exceeds the as-cast foams.

(3) Calculated plateau strengths are notably related to T6 aging treatment in a positive way and decrease with increasing foam densities due to the mixed impact of randomly gap structure of the PEC particles and decreasing volume ratio of porosity.

(4) Heat treatment has a positive effect on the energy absorption capacity. The highest and the lowest energy absorption values of 57.5 and 27.2 MJ·m<sup>-3</sup> are detected for the aging-treated and as-cast foams, respectively.

(5) There is no direct relationship between the aging and densification strain values, and the highest value of 0.65 belongs to as-cast foams, maybe due to the rising ductility of the load-bearing Al metal.

(6) At the beginning of the deformation, as-cast foam samples mainly show ductile-style damage mechanism with the apparent barreling in the foam. However, once the plastic deformation occurs and the strain percentage increases, the samples exhibit a hybrid-type of deformation with some surface and body cracks are found.

(7) While the aging-applied ASFs damage also in a ductile style at the initial parts of the loading, overall, the brittle dominant hybrid-type failure characteristic determines the breakage nature of ASFs. At the end of the compressive loading operation, the aged foams break into many small fragments and their mono block structure deteriorates severely.

## Acknowledgment

The authors thank the Söğüt Toprak Madencilik Sanayi Inc. (Ankara, Turkey) for their fast supply of LECAT® porous expanded clay particles.

## Conflict of interest

The authors declare that they have no conflict of interest.

## References

- [1] Banhart J. Aluminum foams: On the road to real applications. *MRS Bulletin*, 2003, 28(4): 290–295. <https://doi.org/10.1557/mrs2003.832003>
- [2] Birla S, Mondal D P, Das S, et al. Effect of cenosphere particle size and relative density on the compressive deformation behavior of aluminum-cenosphere hybrid foam. *Materials & Design*, 2017, 117: 168–177. <https://doi.org/10.1016/j.matdes.2016.12.078>
- [3] Bolat Ç, Akgün İ C, Gökşenli A. On the way to real applications: Aluminum matrix syntactic foams. *European Mechanical Science*, 2020, 4(3): 131–141. <https://doi.org/10.26701/ems.703619>
- [4] Zhang X T, Wang R Q, Li X G, et al. Energy absorption performance of open-cell aluminum foam and its application in landing buffer system. *Journal of Materials Engineering and Performance*, 2021, 30: 6132–6145. <https://doi.org/10.1007/s11665-021-05823-z>
- [5] Orbulov I N and Szlancsik A. On the mechanical properties of aluminum matrix syntactic foams. *Advanced Engineering Materials*, 2018, 20: 1–12. <https://doi.org/10.1002/adem.201700980>
- [6] Luong D D, Strbik III O M, Hammond V H, et al. Development of high performance lightweight aluminum alloy/SiC hollow sphere syntactic foams and compressive characterization at quasi-static and high strain rates. *Journal of Alloys and Compounds*, 2013, 550: 412–422. <https://doi.org/10.1016/j.jallcom.2012.10.171>
- [7] Padnuru S A, Handjaja C, Manakari V, et al. Development of lightweight magnesium/glass micro balloon syntactic foams using microwave approach with superior thermal and mechanical properties. *Metals*, 2021, 11(5): 827. <https://doi.org/10.3390/met11050827>
- [8] Thiyagarajan R, Senthil K M. Enhanced electromagnetic interference shielding effectiveness of an eco-friendly cenosphere-filled aluminum matrix syntactic foam. *Journal of Electronic Materials*, 2022, 51: 6951–6963. <https://doi.org/10.1007/s11664-022-09925-9>
- [9] Szlancsik A, Katona B, Májlínger K, et al. Compressive behavior and microstructural characteristics of iron hollow sphere filled aluminum matrix syntactic foams. *Materials*, 2015, 8(11): 7926–7937. <https://doi.org/10.3390/ma8115432>
- [10] Orbulov I N, Szlancsik A, Kemény A, et al. Low-cost lightweight composite metal foams for transportation applications. *Journal of Materials Engineering and Performance*, 2022, 31: 6954–6961. <https://doi.org/10.1007/s11665-022-06644-4>
- [11] Bolat Ç, Bekar C, Gökşenli A. Mechanical and physical characteristics of bubble alumina reinforced aluminum syntactic foams made through recyclable pressure infiltration technique. *Gazi University Journal of Science*, 2022, 35(1): 184–196. <https://doi.org/10.35378/gujs.855321>
- [12] Chaves I A, Taherishargh M, Fiedler T. Long-term immersion exposure of perlite-aluminum syntactic foam in seawater. *Journal of Composite Materials*, 2019, 53(9): 1229–1240. <https://doi.org/10.1177/0021998318796264>
- [13] Bolat Ç, Akgün İ C, Gökşenli A. Effects of particle size, bimodality and heat treatment on mechanical properties of pumice reinforced aluminum syntactic foams produced by cold chamber die casting. *China Foundry*, 2021, 18(6): 529–540. <https://doi.org/10.1007/s41230-021-1133-4>
- [14] Kádár C, Chmelík F, Ugi D, et al. Damage characterization during compression in a perlite-aluminum syntactic foam. *Materials*, 2019, 12(20): 3342. <https://doi.org/10.3390/ma12203342>
- [15] Katona B and Orbulov I N. Structural damages in syntactic metal foams caused by monotone or cyclic compression. *Periodica Polytechnica Mechanical Engineering*, 2017, 61(2): 146–152. <https://doi.org/10.3311/PPme.10346>
- [16] Thalmaier G, Sechel N A, Csapai A, et al. Aluminum perlite syntactic foams. *Materials*, 2022, 15(15): 5446. <https://doi.org/10.3390/ma15155446>
- [17] Movahedi N, Fiedler T, Taşdemirci A, et al. Impact loading of functionally graded metal syntactic foams. *Materials Science and Engineering: A*, 2022, 839: 142831. <https://doi.org/10.1016/j.msea.2022.142831>
- [18] Akgün İ C, Bolat Ç, Gökşenli A. Effect of aging heat treatment on mechanical properties of expanded glass reinforced syntactic metal foam. *Kovove Mater.*, 2021, 59(6): 345–355. [https://doi.org/10.4149/km\\_2021\\_6\\_345](https://doi.org/10.4149/km_2021_6_345)
- [19] Rao D W, Yang Y W, Huang Y, et al. Microstructure and compressive properties of aluminum matrix syntactic foams containing Al<sub>2</sub>O<sub>3</sub> hollow particles. *Kovove Mater.*, 2020, 58(6): 395–407. [https://doi.org/10.4149/km\\_2020\\_6\\_395](https://doi.org/10.4149/km_2020_6_395)
- [20] Movahedi N, Murch G E, Belova I V, et al. Effect of heat treatment on the compressive behavior of zinc alloy ZA27 syntactic foam. *Materials*, 2019, 12(5): 792. <https://doi.org/10.3390/MA12050792>
- [21] Balch D K, O'Dwyer J G, Davis G R, et al. Plasticity and damage in aluminum syntactic foams deformed under dynamic and quasi-static conditions. *Materials Science and Engineering: A*, 2005, 391(1–2): 408–417. <https://doi.org/10.1016/j.msea.2004.09.012>
- [22] Santa M J A, Schultz B F, Ferguson J B, et al. Al-Al<sub>2</sub>O<sub>3</sub> syntactic foams – Part I: Effect of matrix strength and hollow sphere size on the quasi-static properties of Al-A206/Al<sub>2</sub>O<sub>3</sub> syntactic foams. *Materials Science and Engineering: A*, 2013, 582: 415–422. <https://doi.org/10.1016/j.msea.2013.05.081>
- [23] Mondal D P, Majumder J D, Jha N, et al. Titanium-cenosphere syntactic foam made through powder metallurgy route. *Materials and Design*, 2012, 34: 82–89. <https://doi.org/10.1016/j.matdes.2011.07.055>
- [24] Xue X and Zhao Y. Ti matrix syntactic foam fabricated by powder metallurgy: Particle breakage and elastic modulus. *The Journal of the Minerals, Metals & Materials Society*, 2011, 63: 43–47. <https://doi.org/10.1007/s11837-011-0027-0>

- [25] Cho Y J, Lee T S, Lee W, et al. Preparation and characterization of iron matrix syntactic foams with glass microspheres via powder metallurgy. *Metals and Materials International*, 2019, 25: 794–804. <https://doi.org/10.1007/s12540-018-00215-w>
- [26] Sánchez de la M A M, García C L E, Malheiros L F, et al. New aluminum syntactic foam: Synthesis and mechanical characterization. *Materials*, 2022, 15(15): 5320. <https://doi.org/10.3390/ma15155320>
- [27] Taherishargh M, Belova I V, Murch G E, et al. Low-density expanded perlite-aluminium syntactic foam. *Materials Science and Engineering: A*, 2014, 604: 127–134. <https://doi.org/10.1016/j.msea.2014.03.003>
- [28] ISO 13314-2011. Mechanical testing of metals-ductility testing-compression test for porous and cellular metals. International Organization for Standardization: Geneva.
- [29] Gupta N, Luong D D, Cho K. Magnesium matrix composite foams—density, mechanical properties, and applications. *Metals*, 2012, 2(3): 238–252. <https://doi.org/10.3390/met2030238>
- [30] Mondal D P, Goel M D, Upadhyay V, et al. Comparative study on microstructural characteristics and compression deformation behaviour of alumina and cenosphere reinforced aluminum syntactic foam made through stir casting technique. *Transactions of the Indian Institute of Metals*, 2018, 71: 567–577. <https://doi.org/10.1007/s12666-017-1211-x>
- [31] Palmer R A, Gao K, Doan T M, et al. Pressure infiltrated syntactic foams—Process development and mechanical properties. *Materials Science and Engineering: A*, 2007, 464(1–2): 85–92. <https://doi.org/10.1016/j.msea.2007.01.116>
- [32] Bolat Ç, Akgün İ C, Gökşenli A. Influences of reinforcement size and artificial aging on the compression features of hybrid ceramic filled aluminum syntactic foams. *Proceedings of the Institution of Mechanical Engineers, Part C: Journal of Mechanical Engineering Science*, 2022, 236(14): 8027–8037. <https://doi.org/10.1177/09544062221083208>
- [33] ASM Handbook. Vol. 4: Heat Treating, ASM Handbook Committee, 1991: 841–879.
- [34] Fiedler T, Al-Sahlani K, Linul P A, et al. Mechanical properties of A356 and ZA27 metallic syntactic foams at cryogenic temperature. *Journal of Alloys and Compounds*, 2020, 813: 152181. <https://doi.org/10.1016/j.jallcom.2019.152181>